Atmos. Chem. Phys. Discuss., doi:10.5194/acp-2016-420, 2016
Manuscript under review for journal Atmos. Chem. Phys.
Published: 8 August 2016

Atmospheric Chemistry and Physics Discussions

The surface aerosol optical properties in urban areas of Nanjing, west Yangtze River Delta of China

B. L. Zhuang[1, 3, *], T. J. Wang[1, 3,**], J. Liu[1, 2, 3], S. Li[1, 3], M. Xie[1, 3], Y. Han[1, 3], P. L. Chen[1], Q. D. Hu[1], X. Q. Yang[1, 3], C. B. Fu[1, 3], J. L. Zhu[4]

[1] School of Atmospheric Sciences, Nanjing University, Xianlin Ave. 163, Nanjing 210023, China

[2] Department of Geography and Planning, University of Toronto, Toronto, M5S 3G3, Canada

[3] Collaborative Innovation Center of Climate Change, Jiangsu Province, China

[4] Department of Energy and Environment, Zhejiang Prov. Development Planning & Research Institute, Hangzhou 310012, China

[*] Corresponding author, E-mail: blzhuang@nju.edu.cn; Tel.: +862589681156; fax: +862589683797

[**] Corresponding author, E-mail: tjwang@nju.edu.cn; Tel.: +862589683797; fax: +862589683797

Abstract: Observational studies of aerosol optical properties are useful to reducing uncertainties in estimating aerosol radiative forcing and forecasting visibility. In this study, the observed near-surface aerosol optical properties in urban Nanjing are analyzed from Mar 2014 to Feb 2016. Results show that near-surface urban aerosols in Nanjing are mainly from local emissions and the regions around. They have lower loadings but are more scattering than in most cities in China. The annual mean aerosol extinction coefficient (EC), single scattering albedo (SSA) and asymmetry parameter (ASP) at 550 nm are 381.96 Mm^{-1}, 0.9 and 0.57, respectively. The aerosol absorption coefficient (AAC) is about one order of magnitude smaller than its scattering coefficient (SC). However, the absorbing aerosol has larger Ångström exponent (AAE) value, 1.58 at 470/660 nm, about 0.2 larger than the scattering aerosols' (SAE). All the aerosol optical properties followed a near unimodal pattern, the ranges around their averages accounting for more than 60% of the total samplings. Additionally, they have substantial seasonality and diurnal variations. High levels of SC and AAC all appear in winter due to higher

Atmos. Chem. Phys. Discuss., doi:10.5194/acp-2016-420, 2016
Manuscript under review for journal Atmos. Chem. Phys.
Published: 8 August 2016

Atmospheric Chemistry and Physics Discussions

aerosol and trace gas emissions. AAE (ASP) is the smallest (largest) in summer because of high relative humidity (RH) which also causes considerably larger SC and smaller SAE, although intensive gas-to-particle transformation could produce a large number of finer scattering aerosols in this season. Seasonality of EC is different from the columnar aerosol optical depth. Larger AACs appear at the rush hours of the day while SC and Bsp only peak in the early morning. Aerosols are fresher at daytime than at nighttime, leading to their larger AE and smaller ASP. Different temporal variations between AAC and SC cause the aerosols more absorbing (smaller SSA) in autumn and around rush hours. ASP has a good quasi-LogNormal growth trend with increasing SC when RH is below 60%. The correlation between AAC and SC at the site is close but a little smaller than that in suburban Nanjing in spring. Atmospheric visibility decreases exponentially with increasing EC or SC, more sharply in spring and summer. It could be further deteriorated with increasing SSA and ASP.

1 Introduction

Atmospheric aerosols have substantial influences on human health, air quality and climate changes and their loadings have significantly increased since the preindustrial times. Due to their ability of scattering/absorbing solar radiation and acting as cloud condensation nuclei, atmospheric aerosols can affect atmospheric radiation and dynamics, as well as the Earth's hydrologic cycle, leading to regional or global climate changes (Forster et al., 2007). Light scattering aerosols have contributed to offsetting the warming effect of CO_2 (Kiehl and Briegleb 1993) while light absorbing aerosols such as black carbon (BC) could further enhance the global warming (Jacobson 2002), especially in the high aerosol regions. Due to the warming effect of BC, the atmosphere would become more unstable, which might result in the changes in the trend of precipitation in China over the past decades as suggested by Menon

Atmos. Chem. Phys. Discuss., doi:10.5194/acp-2016-420, 2016
Manuscript under review for journal Atmos. Chem. Phys.
Published: 8 August 2016

Atmospheric Chemistry and Physics Discussions

et al. (2002). Furthermore, atmospheric aerosols can be a major component in haze pollution, altering atmospheric visibility and being harmful to human health (Chameides and Bergin, 2002).

Observations and modeling studies have been conducted on aerosol optical properties and radiative forcing, as well as its climate effects on regional and global scales in the past two decades (e.g., Penner et al., 2001; Bellouin et al., 2003; Liao and Seinfeld, 2005; Yan et al., 2008; Wu et al., 2012; Zhuang et al., 2013a; 2014a; Wang et al., 2015; Yu et al., 2016). Forster et al. (2007) summarized that large uncertainties exist in estimating the aerosol radiative forcing, especially in climate models. The simulated global mean direct radiative forcing ranged from +0.04 to -0.63 W m^{-2} for total aerosols and from +0.1 to +0.3 W m^{-2} for BC. This would further lead to much larger uncertainties in the estimations of the aerosol climate effects. In East Asia, the range of simulated BC direct raidative forcing is much larger than the global one, varying from +0.32 to +0.81 W m^2 (Zhuang et al., 2013a). The bias is mostly resulted from the uncertainties in the simulated aerosol optical properties (Holler et al., 2003), which, in turn, are related to the aerosol loadings, profiles, compositions, mixing states and the atmospheric humidity. The uncertainty could be substantially reduced in a model if the aerosol optical properties are corrected based on the observations or if the observed properties are directly used (Forster et al., 2007).

In the last three decades, China has experienced the rapidest economic growth among East Asia and even the world. This leads to high emission of aerosols and trace gases (Zhang et al., 2009). The anthropogenic aerosol emissions in East Asia were estimated to exceed 1/4 of the global emissions (Streets et al., 2001), resulting in more diversified aerosol compositions, complex species and heterogeneous spatial distributions in the region (Zhang et al., 2012), especially in megacities and urban agglomerations (e.g., Beijing-Tianjin-Hebei (BTH), Yangtze River Delta (YRD) and Pearl River

Atmos. Chem. Phys. Discuss., doi:10.5194/acp-2016-420, 2016
Manuscript under review for journal Atmos. Chem. Phys.
Published: 8 August 2016

Atmospheric Chemistry and Physics Discussions

Delta (PRD) regions). Uncertainties in the aerosol radiative forcing and corresponding climate effects might be much larger than in the rest of the world. Therefore, it is necessary to characterize the aerosol optical properties based on observations in China, as did many studies in recent years at urban sites and in rural areas (e.g., Bergin et al., 2001; Xu et al., 2002; 2004; Zhang et al., 2004; Yan, 2006; Xia et al., 2007; Li et al., 2007; Yan et al., 2008; Andreae et al., 2008; He et al., 2009; Wu et al., 2009; Wang et al., 2009; Li et al., 2010; Fan et al., 2010; Bai et al., 2011; Cai et al., 2011; Xiao et al., 2011; Xu et al., 2012; Wu et al., 2012; Zhuang et al., 2015; Zhang et al., 2015; Li et al., 2015a; b; Yu et al., 2016). In urban areas, Bergin et al. (2001) reported that the monthly mean aerosol scattering coefficient (SC at 530 nm) and absorption coefficient (AAC at 565 nm) were 488 and 83 Mm^{-1}, respectively, near the surface in Beijing in June 1996. The annual mean 532 nm-AAC in Beijing was about 56 Mm^{-1} from 2005 to 2006 (He et al. 2009) and it was 41~44 Mm^{-1} in an urban site of YRD from 2012 to 2013 (Zhuang et al., 2015). Observations from Wu et al. (2009), Cao et al. (2012) and Tao et al. (2014) suggested that the annual averaged aerosol optical properties were much larger in center to southwest China and in PRD. The annual mean 520 nm-SC and 532 nm-AAC were 525 and 83 Mm^{-1}, respectively, in Xi'an in 2009 and were 456 and 96 Mm^{-1}, respectively, in Chengdu in 2011. AAC was about 82 ± 23 Mm^{-1} in PRD. In rural and other areas, Xu et al. (2002; 2004) showed that 530 nm-SC and 565 nm-AAC were 353 and 23 Mm^{-1}, respectively, at a rural site in YRD in Nov 1999, and were 158 and 6 Mm^{-1}, respectively in desert region (Yulin) in Apr 2001. Yan et al. (2008) reported that the annual mean 532 nm-AAC and 525 nm-SC from 2003 to 2005 were 17.5 and 174.6 Mm^{-1}, respectively, at a rural site in Beijing. In addition to surface measurements, the columnar optical properties of the aerosols were also observed. Xia et al. (2007) indicated that the annual mean aerosol optical depth (AOD) at 500 nm and its Ångström exponent (AE) in YRD were about 0.77 and 1.17, respectively.

Atmos. Chem. Phys. Discuss., doi:10.5194/acp-2016-420, 2016
Manuscript under review for journal Atmos. Chem. Phys.
Published: 8 August 2016

Atmospheric Chemistry and Physics Discussions

Zhuang et al. (2014a) suggested that the AOD and AE of absorbing aerosols from 2011 to 2012 were 0.04±0.02 and 1.44±0.50, respectively, in urban Nanjing. Che et al. (2015) reported long-term measurements of the countrywide-aerosol optical depths and Ångström exponents in China from 2002 to 2013. In spite of substantial observation-based studies mentioned, measurements and analysis on aerosol properties in YRD region, one of the most populous regions in China, is still rather limited. To fill the gaps in the current observational network in China and to better understand the optical properties of urban aerosols in YRD, this study will analyze the observations of aerosol scattering (SC), back scattering (Bsp), absorption (AAC), extinction (EC) coefficients and single scattering albedo (SSA), Ångström exponent of scattering (SAE) and absorbing (AAE) aerosols, as well as aerosol asymmetry parameter (ASP) in urban area of Nanjing, a major megacity in YRD. Our ultimate goals are to reduce uncertainties in estimating aerosol radiative forcing and climate effect and to improve forecast accuracy of visibility.

In the following, the method is described in Section 2. Results and discussions are presented in Section 3, followed by Conclusions in Section 4.

2 Methodologies

2.1 Sampling station and instruments

The sampling station is located at the Gulou campus of Nanjing University, urban area of Nanjing (32.05^{o} N, 118.78^{o} E). It is built on the roof of a 79.3 m-tall building, around which there are no industrial pollution sources within a 30-km radius but there are several main roads with apparent traffic pollution, especially at rush hours. The layout of the site and the corresponding climatology have been described in Zhu et al. (2012).

Atmos. Chem. Phys. Discuss., doi:10.5194/acp-2016-420, 2016
Manuscript under review for journal Atmos. Chem. Phys.
Published: 8 August 2016

Atmospheric Chemistry and Physics Discussions

113 The wavelength dependent aerosol absorption coefficient (AAC) and concentrations of black
114 carbon (BC) were derived from the measurements using a seven-channel Aethalomter (model AE-31,
115 Magee Scientific, USA). The wavelength dependent aerosol scattering coefficient (SC) and back
116 scattering coefficient (Bsp) were measured by a three-wavelength integrating Nephelometer (Aurora
117 3000, Australia). To make a brief comparison, the wavelength dependent columnar aerosol optical
118 depth (AOD) was observed using a Cimel sunphotometer (CE-318). The AE-31 model measures light
119 attenuation at seven wavelengths, including 370, 470, 520, 590, 660, 880, and 950 nm, respectively,
120 with a desired flow rate of 5.0 L/min and a sampling interval of 5 min. Aurora 3000 measures the
121 aerosol's light scattering, including SC and Bsp at 450, 525 and 635 nm, with a sampling interval of 1
122 min. CE-318 measures the AOD from 340 to 1640 nm at day times. Routine calibrations and
123 maintenances were carried out for all these instruments during the sampling periods. R-134 was used as
124 a span gas for Aurora 3000. The aerosol inlet is located about 1 m above the roof. Data to be analyzed
125 in this study were measured from Mar 2014 to Feb 2016 for AE-31 and CE-318 and from Jun 2014 to
126 Feb 2016 for Aurora 3000. Meteorological data during the sampling period are from the National
127 Meteorological Station of Nanjing (No. 58238).
128
129 **2.2 Calculation of the aerosol optical properties**
130 The wavelength dependent aerosol absorption coefficient (AAC) and BC mass concentration
131 can be calculated directly based on the measured light attenuations through a quartz filter matrix
132 (Petzold et al., 1997; Weingartner et al., 2003; Arnott et al., 2005; Schmid et al., 2006):

133 $$\sigma_{\mathrm{ATN},t}(\lambda) = \frac{(\mathrm{ATN}_t(\lambda) - \mathrm{ATN}_{t-1}(\lambda))}{\Delta t} \times \frac{A}{V} \quad (1)$$

134 where A (in m^2) is the area of the aerosol-laden filter spot, V is the volumetric sampling flow rate (in

Atmos. Chem. Phys. Discuss., doi:10.5194/acp-2016-420, 2016
Manuscript under review for journal Atmos. Chem. Phys.
Published: 8 August 2016

Atmospheric Chemistry and Physics Discussions

L/min) and Δt is the time interval (=5 min) between *t* and *t-1*. σ_{ATN} is the AAC without any correction, which is generally larger than the actual one (σ_{abs}) because of the optical interactions of the filter substrate with the deposited aerosol. Generally, there are two key factors leading to the bias: 1) multiple scattering of light at the filter fibers (multiple scattering effect), and 2) instrumental response with increased particle loading on the filter (shadowing effect). Thus, the correction is needed and the calibration factors *C* and *R* (shown in Eq. 2) are introduced to against the scattering effect and shadowing effect, respectively:

$$\sigma_{abs,t}(\lambda) = \frac{\sigma_{ATN,t}(\lambda)}{C \times R} \quad (2)$$

Collaud Coen et al. (2010) suggested that AAC corrected from Weingartner et al. (2003) (WC2003 for short, hereinafter) and Schmid et al. (2006) (SC2006 for short, hereinafter) have good agreements with the one measured by a Multi-Angle Absorption Photometer. These two corrections are similar to each other and they use the same $R(\lambda)$:

$$R_t(\lambda) = (\frac{1}{f} - 1) \times \frac{\ln(ATN_t(\lambda)) - \ln 10}{\ln 50 - \ln 10} + 1 \quad (3)$$

where R =1 when $ATN \le 10$ and f =1.2. However, C value is fixed in WC2003 while is wavelength dependent in SC2006. According to Wu et al. (2013) and Zhuang et al. (2015), C in Nanjing is 3.48 in WC2003 while it is 2.95, 3.37, 3.56, 3.79, 3.99, 4.51 and 4.64 at 370, 470, 520, 590, 660, 880, and 950 nm, respectively, in SC2006. Zhuang et al. (2015) further suggested that wavelength dependent AACs corrected by SC2006 might be more close to the real ones than WC2003's in Nanjing, although 532 nm-AACs from these two corrections are close to each other. In addition to the direct way, AAC can also be calculated indirectly:

$$\sigma_{abs,t}(\lambda) = [BC] \times \gamma \quad (4)$$

Atmos. Chem. Phys. Discuss., doi:10.5194/acp-2016-420, 2016
Manuscript under review for journal Atmos. Chem. Phys.
Published: 8 August 2016

Atmospheric Chemistry and Physics Discussions

where [BC] is the mass concentration of Aethalometer BC (in μg/m^3) without any correction and γ is the conversion factor determined empirically from linear regression of the Aethalometer BC concentration versus the aerosol absorption measurement (Yan et al., 2008). Zhuang et al. (2015) indicated that γ from the linear regression of the Aethalometer BC concentrations (ng/m^3) at 880 nm against the light absorption coefficient (Mm^{-1}) at 532 nm in Nanjing is about 11.05 m^2/g. It's obviously that only 532 nm-AAC can be addressed from this way. Thus, AACs corrected from SC2006 are used in this study.

Based on wavelength dependent AAC and SC, Ångström exponent of scattering (SAE) and absorbing (AAE) aerosols are estimated as followed:

$$AAE_{470/660\mathrm{nm}} = -\log(AAC_{470nm} / AAC_{660nm}) / \log(470/660) \quad (5)$$

$$SAE_{450/635\mathrm{nm}} = -\log(SC_{450nm} / SC_{635nm}) / \log(450/635) \quad (6)$$

For purposes of comparison, AAC at 450, 525, 532, 550 and 635 nm, SC at 532 and 550 nm as well as Bsp at 532 and 550 nm were further calculated by the given coefficients and corresponding Ångström exponents:

$$\sigma_\lambda = \sigma_{\lambda_0} \times (\frac{\lambda}{\lambda_0})^{-\alpha} \quad (7)$$

where, σ_λ is the coefficient at wave length λ, α is the corresponding Ångström exponents.

Based on wavelength dependent SC, Bsp, AAC, aerosol asymmetry parameter (ASP), single scattering albedo (SSA) and extinction coefficient (EC) are further estimated:

$$ASP_\lambda = -7.143889\beta_\lambda^3 + 7.46443\beta_\lambda^2 - 3.9356\beta_\lambda + 0.9893 \quad (8)$$

$$SSA_\lambda = \frac{SC_\lambda}{SC_\lambda + AAC_\lambda} \quad (9)$$

$$EC_\lambda = SC_\lambda + AAC_\lambda \quad (10)$$

Atmos. Chem. Phys. Discuss., doi:10.5194/acp-2016-420, 2016
Manuscript under review for journal Atmos. Chem. Phys.
Published: 8 August 2016

where, β_λ is the ratio of Bsp to SC at wavelength λ. Eq. 8 derives from Andrews et al. (2006).

3 Results and discussions

It's well known that the temporal variations of the aerosol optical properties at different wavelengths are generally consistent with each other. Therefore, only single wavelength (such as 550 nm) AAC, SC, Bsp, SSA and ASP are focused when analyzing their basic characteristics (including temporal variations, frequency distributions and changes with wind direction), their relationships with each other, and their relationships with the meteorological conditions (such as RH and VIS) and columnar AOD.

3.1 Temporal variations of the aerosol optical properties

The aerosol absorption coefficient (AAC) was directly obtained from the measurement of AE-31 and the scattering and back scattering coefficients (SC and Bsp) were directly measured from Aurora 3000. Based on wavelength dependent AAC and SC, Ångström exponent of absorbing (AAE at 470/660 nm) and scattering (SAE at 450/635 nm) aerosols were estimated according Eq.5 and Eq. 6, respectively. Based on AAC, SC and Bsp, wavelength dependent aerosol asymmetry parameter (ASP), single scattering albedo (SSA) and extinction coefficient (EC) are further estimated using Eq. 8~10 and analyzed. Table 1 lists the statistical summary of surface aerosol optical properties in urban area of Nanjing during the sampling period. The annual mean AAC, SC, Bsp, EC, SSA and ASP at 550 nm, AAE at 470/660 nm and SAE at 450/635 nm is 29.615 Mm^{-1}, 338.275 Mm^{-1}, 44.257 Mm^{-1}, 381.958 Mm^{-1}, 0.901, 0.571, 1.583 and 1.320, respectively, with a standard deviation of 20.454 Mm^{-1}, 228.078 Mm^{-1}, 27.396 Mm^{-1}, 252.271 Mm^{-1}, 0.049, 0.088, 0.228 and 0.407, respectively.

Table 1

Atmos. Chem. Phys. Discuss., doi:10.5194/acp-2016-420, 2016
Manuscript under review for journal Atmos. Chem. Phys.
Published: 8 August 2016

Atmospheric Chemistry and Physics Discussions

Figure 1 shows the 10th, 25th, median, 75th and 90th percentile values of the 550 nm- AAC, SC, Bsp, 470/660 nm-AAE and 450/635 nm-SAE in urban area of Nanjing in each season from Mar 2014 to Feb 2016. Default values of the scattering aerosols' optical properties in spring 2014 are blank because the measurements of Aurora 3000 started from June 2014. The figure suggests that AAC, SC, Bsp, AAE and SAE have substantially seasonal variations. High level of AAC appears in winter times (DJF) while the lower one is found in summer (JJA) (Fig. 1a). The temporal trend of Bsp is similar to AAC's (Fig. 1d). According to Zhang et al. (2009), emissions of the aerosols and trace gases in China are larger in winter than in the other seasons especially for carbonaceous aerosols (Fig. 1c in Zhuang et al., 2013b). Thus, the higher AAC values in winter than in summer might be mostly resulted from the higher aerosol emissions, lower boundary height and less rainfall. However, possibly due to the impacts of RH in summer and dust aerosol in spring (Zhuang et al., 2014a), SC is considerably large in these two seasons (Fig. 1c). Thus, the lowest SC is found in autumn in both 2014 and 2015. AAE has seasonality similar to AAC. Due to RH, small value of AAE is found in JJA while the larger ones appear in the other seasons (Fig. 1b), which is different from the seasonality of SAE. SAE is larger in warmer seasons but is smaller in the other seasons. Scattering aerosols, including inorganic and partially organic components, mainly come from gas-to-particle transformation, so that they have smaller sizes (larger AE) compared to the primary aerosols (such as dust and BC). The efficiency of gas-to-particle transformation is higher in warmer seasons. The observations of the aerosol compositions at the site showed that seasonal mean inorganic aerosols, including sulfate, nitrate and ammonium, account for about 50% of the total $PM_{2.5}$ in spring and might be higher than 50% in the other seasons (Zhuang et al., 2014b). Thus, SAE in summer and autumn is large (Fig. 1e). RH can impose substantial influences on scattering aerosols. SAE might be much larger than the current values

Atmos. Chem. Phys. Discuss., doi:10.5194/acp-2016-420, 2016
Manuscript under review for journal Atmos. Chem. Phys.
Published: 8 August 2016

in these two seasons if the moisture absorption growing were excluded. Seasonal mean RH is about 75.41% and 70.86% in JJA and SON, respectively, to a certain degree leading to higher values of SAE in autumn than in summer. The figure also suggests that aerosol absorption coefficient and scattering coefficient as well as their sizes in 2014 are higher than those in 2015, which might somewhat relate to a difference in RH in these two years. A comparison of RH between 2014 and 2015 indicates that RH is 79.49% and 72.86% in JJA and SON, respectively, in 2014, larger than that in 2015 (71.33% in JJA and 69.03 in SON).

Figure 1

Figure 2 plots the seasonal mean values with standard deviations of AAC, SC, Bsp, EC, SSA, ASP at four wavelengths, AAE at 470/660 nm and SAE at 450/635 nm. AAC, SC, Bsp and EC increase with decreasing wavelength in four seasons. Changes in SSA and ASP with increasing wavelength are different in different seasons. SSA increases with increasing wavelength in colder seasons but little in JJA and SON. ASP increases with wavelength in JJA, opposite to in other seasons. The figure also suggests that seasonal variation of EC is more consistent with SC's, with large values in JJA and DJF (370.236 and 422.569 Mm^{-1}, respectively, at 550 nm). The largest values of SSA and ASP appear in JJA (0.933 and 0.638, respectively, at 550 nm), implying that aerosols in urban area of Nanjing are more scattering and have stronger forward scattering ability in JJA than in other seasons. The urban aerosols are more absorbent in SON in Nanjing (550 nm SSA is about 0.874).

Figure 2

Seasonal mean 550 nm AAC, SC, Bsp, EC, SSA, and ASP, 470/660 nm AAE and 450/635 nm SAE as well as corresponding standard deviations are listed in Table 2. It suggests that seasonal mean 550 nm AAC, SC, Bsp, EC, SSA, and ASP vary from 19.65 to 37.96 Mm^{-1}, 294.62 to 385.14 Mm^{-1},

Atmos. Chem. Phys. Discuss., doi:10.5194/acp-2016-420, 2016
Manuscript under review for journal Atmos. Chem. Phys.
Published: 8 August 2016

Atmospheric Chemistry and Physics Discussions

36.99 to 54.79 Mm^{-1}, 341.3 to 422.57 Mm^{-1}, 0.874 to 0.933, and 0.54 to 0.64, respectively. Seasonal mean AAE and SAE vary from 1.49 to 1.70 and 1.1 to 1.54, respectively. AAC and Bsp in DJF are about 2 and 1.5 times of those in JJA, respectively. SSA in JJA is about 6.75% larger than that in SON.

Table 2

In addition to seasonality, the aerosol optical properties near the surface at urban Nanjing have substantial diurnal variations (Figure 3), especially for the coefficients (AAC, SC, Bsp and EC). The diurnal variation of EC, which is consistent with SC, is not showed in the figure. AAC levels are usually high at the rush hours around 07:00-09:00 am and around 09:00-11:00 pm but low in the afternoon (Fig. 3a). At 08:00 am, mean 550 nm-AAC is as large as about 34 Mm^{-1}, while at 02:00 pm, it is about 23 Mm^{-1}. SC and Bsp (Fig. 3b and 3c), to some extent, have diurnal variations similar to AAC's. Their lowest values also appear in the afternoon (about 280 Mm^{-1} for SC and 38 Mm^{-1} for Bsp). However, only one peak of the aerosol scattering coefficient is found in the early morning (about 379 Mm^{-1} for Sc and 48 Mm^{-1} for Bsp) and it is about 1-2 hours earlier than its absorption coefficient possibly owing to the different emissions between these two types of aerosols. Absorbing aerosols in urban Nanjing mainly come from the vehicle emissions because of the developed transportation network, resulting in two peaks of AAC within one day (Zhuang et al. 2015). Scattering aerosol loadings are somewhat less affected by traffic emissions especially in nighttime. Their precursors, such as SO_2 and NOx, are mostly come from coal combustion and industrial emissions in urban Nanjing based on source apportionment. Therefore, there is no peak for SC or Bsp before midnight, although their values are considerably large (about 350 and 46 Mm^{-1}, respectively). Different diurnal cycles between AAC and SC were also observed in sub-urban area of Nanjing (Yu et al., 2016). Diurnal variations of AAC, SC and Bsp might be highly affected by the diurnal cycles of the boundary layer.

Atmos. Chem. Phys. Discuss., doi:10.5194/acp-2016-420, 2016
Manuscript under review for journal Atmos. Chem. Phys.
Published: 8 August 2016

265 The small coefficients in afternoon are mostly induced by well developed mixing layer (Zhuang et al.
266 2014b). Generally, the boundary layer becomes more and more stable after sunset and its height
267 becomes lower, which is conducive to the accumulation of air pollutants in the nighttime especially
268 during the period from midnight to sunrise. Therefore, SC usually peaks in early morning and the peak
269 appears at different times in different seasons (05:00 am in JJA and 08:00-09:00 am in DJF). The
270 daytime peak of AAC appears at 07:00 am in JJA and at 09:00 am in DJF. Diurnal variation of SSA
271 also reflects the difference between AAC and SC (Fig. 3d), implying that aerosols in urban Nanjing are
272 more scattering after midnight (SSA is about 0.91) while more absorbing before noon and midnight
273 (SSA is about 0.89). Additionally, SSA is also large in afternoon possibly because the dilution effect of
274 well developed boundary layer on scattering aerosol is weaker than that on absorbing aerosols.
275 Scattering aerosols mainly come from strong chemical production (gas-to-particle transformation) at
276 daytime, which to some extent offsets the dilution effect of the boundary on SC. The figure further
277 shows that both AAE (Fig. 3e) and SAE (Fig. 3f) at daytime are slightly larger than those after
278 midnight because both absorbing and scattering aerosols are more fresher at daytime while they are
279 more aged before sunrise. Diurnal variations of SAE and AAE are relatively weaker compared to
280 corresponding coefficients. In addition to aerosol loadings, the level of Bsp is also affected by the size
281 of the aerosols as suggested by Yu et al. (2016), so is ASP (Fig. 3g). Diurnal cycle of ASP is similar to
282 that of Bsp but is opposite to that of SAE. Large ASP appears in early morning (0.587) and the lower
283 ASP in afternoon (0.552).

284 **Figure. 3**

285 **3.2 Frequencies of the aerosol optical properties**

286 The frequency of the aerosol optical properties is presented in Figure 4. Similarly, the frequency

Atmos. Chem. Phys. Discuss., doi:10.5194/acp-2016-420, 2016
Manuscript under review for journal Atmos. Chem. Phys.
Published: 8 August 2016

Atmospheric Chemistry and Physics Discussions

of EC is not shown in the figure because it has similar pattern to SC's. Almost all of them follow a unimodal pattern. The dominant range is from 9 to 45 Mm^{-1} for AAC, 60 to 390 Mm^{-1} for SC, 15 to 60 Mm^{-1} for Bsp, 0.87 to 0.97 for SSA 1.4 to 1.8 for AAE, 0.96 to 1.68 for SAE and 0.48 to 0.69 for ASP, accounting for over 73%, 67%, 69%, 73%, 71%, 62% and 81% the total samplings during the entire study period, respectively. The maximum frequencies of 32.9% (AAC), 24.04% (SC), 26.45% (Bsp), 18.64% (SSA), 20.9% (AAE), 18.06% (SAE) and 34% (ASP) occur in the ranges from 9 to 21 Mm^{-1}, 170 to 280 Mm^{-1}, 30 to 45 Mm^{-1}, 0.91 to 93, 1.5 to 1.6, 1.32 to 1.5 and 0.55 to 0.62, respectively. Frequency distributions of the aerosol optical properties have substantially seasonal variations. The frequency peaks of the properties would be more concentrated at lower/higher ranges if their seasonal means are smaller/larger. As shown in Fig. 4a, 4c, and 4e, relatively larger values or the peaks of frequencies for AAC, Bsp and AAE are concentrated in lower value ranges in JJA but in higher value ranges in the other seasons. Moisture absorption growth of absorbing aerosols leads to a left-ward shift in an AAE-frequency curve in JJA. Effects of dust aerosol also might result in a left-ward shift in a SC-frequency curve in spring (Fig. 4f). Furthermore, due to dust and RH, SC is considerably large in MAM and JJA, leading to relatively larger frequencies of SC distributed at larger SC ranges compared with the ones of AAC. As mentioned above, aerosols in urban Nanjing are more scattering and have stronger forward scattering ability in JJA than in the other seasons, thus larger frequencies occur more at higher value ranges of SSA and ASP in JJA.

Figure 4

3.3 Aerosol optical properties in different wind directions

East Asian monsoon is active in middle latitudes. Nanjing could be affected by East Asian summer monsoon in JJA and by the winter monsoon in DJF. Air flows in these two seasons are significantly

Atmos. Chem. Phys. Discuss., doi:10.5194/acp-2016-420, 2016
Manuscript under review for journal Atmos. Chem. Phys.
Published: 8 August 2016

Atmospheric Chemistry and Physics Discussions

309 different (Figure 5a and 5b) so to alter the aerosol optical properties in different seasons. Air masses
310 mostly come from the oceans (about 77%) in JJA and from continental regions in north and northwest
311 of China (57%) in DJF. Only a few percentages of air masses are from the north region of China in JJA.
312 Additionally, considerable air masses arriving at the site are from the local areas (cluster 1 in JJA) or
313 from places near Nanjing (cluster 1 in DJF). Therefore, the aerosol optical properties at the study site
314 are characterized differently with different air masses in the two seasons.

315 As suggested by Zhuang et al. (2014b), high BC loadings in early June 2012 were observed at the
316 site when the air masses were from northwestern directions of Nanjing, in which seriously biomass
317 burning was detected. Therefore, the aerosol optical properties are further analyzed by their origins in
318 both JJA and DJF (Fig 5c and 5d). In JJA, seasonal mean AAC, SC, Bsp, SSA, ASP, AAE and SAE are
319 about 19.65 Mm^{-1}, 340.87 Mm^{-1}, 36.99 Mm^{-1}, 0.93, 0.64, 1.49 and 1.34, respectively. The dominant air
320 masses are from local areas (cluster 1 in Fig. a) and east ocean (on the way through urban
321 agglomeration regions (cluster 2) and less-developed regions (cluster 3) of the Yangtze River Delta
322 YRD), accounting for 90% of the total characteristics of the aerosol optical properties in urban Nanjing.
323 All the values of the properties in the first three clusters are more close to their season means. Aerosol
324 absorption and scattering coefficients from local emissions are larger than those in the other clusters.
325 Although air masses in cluster 2 and cluster 3 come from the oceans and have the same level of relative
326 humidity (RH), differences still exist between the clusters. The air masses have to cross the urban
327 agglomeration (from Shanghai to Nanjing) of YRD when they arrive Nanjing in cluster 2 but pass less
328 developed regions (north Jiangsu Province) in cluster 3. In YRD, emissions of the aerosols and trace
329 gases are much stronger in urban agglomeration regions than those in other area as suggested in Zhang
330 et al. (2009) and Zhuang et al. (2013b). Therefore, AAC and SC in cluster 2 are larger than those in

Atmos. Chem. Phys. Discuss., doi:10.5194/acp-2016-420, 2016
Manuscript under review for journal Atmos. Chem. Phys.
Published: 8 August 2016

cluster 3 to some extent (Fig. 5a and 5c). Aerosols from these two clusters are more scattering than the local ones. There are two clusters (cluster 4 and 5 in Fig. 5a) from the remote areas in JJA. Aerosol loadings are relatively small when the air masses from these two clusters. The size of the aerosols is finer (larger AAE in cluster 5 and SAE in cluster 4 and 5 in Fig. 5c). ASP varying with the clusters coincides with RH varying with the clusters (Fig. 5c), implying that RH might influence ASP significantly. In DJF, seasonal mean AAC, SC, Bsp, SSA, ASP, AAE and SAE are about 37.96 Mm^{-1}, 385.14 Mm^{-1}, 54.79 Mm^{-1}, 0.89, 0.54, 1.70 and 1.24, respectively. Similar to JJA, the aerosol absorption and scattering coefficients are the largest, all of which (AAC, SC and Bsp) are about 1.3 times of their season means (Fig. 5d), when the air masses are local or from the regions (cluster 1 in Fig. 5b) near Nanjing in DJF. AAC, SC, Bsp, SSA and ASP are small but AAE and SAE are large if air masses are from remote areas. Aerosols are the smallest, most absorbing and finest when the air masses are from near Lake Baikal. ASP varying with the clusters also coincides with RH varying with the clusters in this season (Fig. 5d), further implying the effect of RH on ASP.

Figure 5

Substantial studies on the aerosol optical properties have been carried out in China from monthly to annual scales. Table 3 lists some annual and seasonal statistics of measured surface aerosol optical properties from literature. Annual and season means listed in the table are comparable to some extent, although the observational periods and instruments are different. It suggests that AACs and SCs in urban areas are much higher than those in rural and remote areas. In Beijing (center of Beijing-Tianjin-Hebei region), annual mean AAC and SC were 56 and 288 Mm^{-1} in urban site during the period from 2005 to 2006 (He et al., 2009), which were much larger than the ones (17.5 and 174.6 Mm^{-1}, respectively) in rural area (Yan et al., 2008). In Chengdu (Tao et al., 2014), Xi'an (Cao et al.,

Atmos. Chem. Phys. Discuss., doi:10.5194/acp-2016-420, 2016
Manuscript under review for journal Atmos. Chem. Phys.
Published: 8 August 2016

353 2012) and Wuhan (Gong et al., 2015), which is the center from southwest to central China, the annual
354 mean scattering coefficients in these cities exceeded 450, 520 and 370 Mm^{-1}, respectively. In Pearl
355 River Delta (PRD) region, seasonal mean AAC at 532 nm was about 84 and 188 Mm^{-1} at an urban site
356 (Panyu), about 47 and 95 Mm^{-1} at a suburban site (Dongguan), about 26 and 28 Mm^{-1} at a rural site,
357 and only 7.21 and 8.37 Mm^{-1} at a remote site (Yongxing Island), in spring and winter, respectively (Wu
358 et al., 2013). Additionally, aerosols in urban areas are more absorbing. The aerosol absorptions in urban
359 areas have stronger seasonality than those in rural areas (Table 3). Urban aerosols in Nanjing in annual
360 scale are somewhat lower but more scattering than those in most cities in China. In addition to annual
361 and seasonal means, there are considerable studies on monthly mean aerosol optical properties (e.g.,
362 Bergin et al., 2001; Xu et al., 2002; 2004; Li et al., 2007; Andreae et al., 2008; Li et al., 2015a; b). A
363 few studies on the aerosol optical properties in Nanjing have been carried out previously (Zhuang et al.,
364 2014a; 2015; Yu et al., 2016) based on observations. They were more focused on the columnar aerosols
365 (Zhuang et al., 2014a), or single optical property (Zhuang et al., 2015), or shorten observations (two
366 months in Yu et al., 2016). Substantial analysis in the key optical properties of the surface aerosol here
367 to a certain degree fill the gaps in the study on the aerosols in Nanjing, even in YRD.

368 **Table 3**

369 **3.4 Relationship among aerosol optical properties, relative humidity and visibility**

370 The relationships between SC and AAC, SC and Bsp are presented by season in Figure 6. As
371 shown in Figures 3 and 4, these three types of coefficients have similar diurnal and frequency
372 distributions. It is obviously that relations between SC and Bsp are much better than those between SC
373 and AAC in all seasons. The linear correlation coefficient varies from 0.93 to 0.97 for SC and Bsp and
374 from 0.66 to 0.87 for SC and AAC in urban Nanjing. The correlation between AAC and SC becomes

Atmos. Chem. Phys. Discuss., doi:10.5194/acp-2016-420, 2016
Manuscript under review for journal Atmos. Chem. Phys.
Published: 8 August 2016

Atmospheric Chemistry and Physics Discussions

375 poorer in MAM (0.66) and JJA (0.87) because the scattering aerosols is more affected by dust in spring
376 and SC is more affected by RH in summer. The linear correlation coefficients between SC and AAC
377 and between SC and Bsp in MAM at the site were a little smaller than that in suburban Nanjing (Yu et
378 al., 2016) in the same season in 2011. The slope of the fitting between Bsp and SC represents the levels
379 of ASP. Analysis (not shown) suggests that ASP has a significant anti-correlation with the ratio of Bsp
380 to SC (linear R=-0.98). Thus, a greater slope of curve represents a smaller ASP, thus less forward
381 scattering of the aerosols.

382 **Figure 6**

383 The correlations between ASP and SC under different RH conditions are illustrated in Figure 7,
384 showing that ASP has a quasi-LogNormal distribution with SC especially in lower RH conditions. ASP
385 increases monotonically with increasing SC in low RH ranges (Fig. 7a and 7b, RH < 60%) and ASP
386 mostly concentrates at small SC regions when RH is less than 40% (Fig. 7a), implying that fine
387 particles dominates the most in low RH conditions as also suggested by Andrews et al. (2006) and
388 Badu et al. (2012). The correlation between ASP and SC becomes poorer with increasing RH (Fig. c),
389 indicating that both fine and coarse aerosols might be equally important to the total SC.

390 **Figure 7**

391 Figure 8 shows the relationships between the SSA at 491 nm and extinction Angstrom exponent
392 (EAE) at 491/863 nm (Fig. a) as well as between SSA difference (863 nm - 491 nm) (short for dSSA)
393 and EAE at 491/863 nm (Fig. b). Overall, SSA or dSSA to a certain degree have an anti-correlation
394 with EAE in urban area of Nanjing, especially for the latter one. Linear correlation coefficient is about
395 -0.13 between SSA and EAE and about -0.75 between dSSA and EAE. Relationships between the SSA
396 (or dSSA) and EAE to some extent reflect the aerosol types and sources as indicated by Russell et al.

Atmos. Chem. Phys. Discuss., doi:10.5194/acp-2016-420, 2016
Manuscript under review for journal Atmos. Chem. Phys.
Published: 8 August 2016

(2014), who proposed a method to identify the aerosol types based on the columnar aerosol optical properties (including SSA, EAE and the real refractive index) from the Aerosol Robotic Network (AERONET) retrievals. They suggested that: 1. The polluted dust aerosol had smaller EAE (near 1.0) and SSA ranged from 0.85 to 0.95. 2. The urban aerosols had larger EAE values (around 1.4) and SSA ranges (0.86~1.0) compared with the dust aerosols. 3. The biomass burning aerosol (dark type) had the largest EAE (exceeding 1.5) while smaller SSA (about 0.85). If there were two kind of aerosols having nearly identical coordinates in SSA and EAE, further information (such as the real refractive index) should be used (Russell et al., 2014). Based on this method, the figure further implies that, in addition to local emissions, aerosols in urban area of Nanjing might also be affected substantially by the long distance transported dust (or polluted dust) in spring and be influenced to some extent by biomass burning in fall.

Figure 8

Atmospheric humidity has significant influences on the growth of particulate matter, subsequently affecting the sizes and absorbing/scattering abilities of the aerosols. As shown in Figure 7a and 7c, high levels of SC are likely found in high RH ranges. Seasonal mean RH is the largest in summer but lowest in winter (Figure 9a). Due to the effects of RH in summer, the aerosol scattering efficiency would be enhanced substantially (Fig. 1c). Additionally, the smallest AAE in JJA corresponds to the highest RH, and vice versa (Fig. 1b), indirectly verifying the effects of RH on the size of absorbing aerosols, i.e., coarser in high RH but finer in low RH. These results are consistent with Zhuang et al. (2014a), in which characteristic of columnar aerosol optical properties were investigated. Figure 9b further shows that AAE and SAE decrease monotonically with increasing RH. The correlation between ASP and RH is opposite to that between aerosol Ångström exponent and RH, implying that the forward scattering

Atmos. Chem. Phys. Discuss., doi:10.5194/acp-2016-420, 2016
Manuscript under review for journal Atmos. Chem. Phys.
Published: 8 August 2016

efficiency increases with increasing in RH. The linear correlation coefficients are -0.36, -0.15 and 0.6 between AAE and RH, SAE and RH, and ASP and RH, respectively, in urban areas of Nanjing. The relation between ASP and RH is the best among these three optical properties, which has somewhat shown in Fig. 2f, Fig. 5c and Fig. 5d. These results could be used to correct the aerosol optical parameters in numerical models for estimating the aerosol radiative forcing in East China as suggested by Andrews et al. (2006), in hope to reduce uncertainties in such estimation.

Figure 9

High levels of aerosol loadings would directly affect the visibility (VIS), which is one of the factors being concerned about in current air quality forecasting in China. The forecast accuracy of visibility or haze pollutions would be increased significantly if the effects of aerosols on visibility can be figured out. Instead of the loadings of the particulate matter, the aerosol optical properties here are used when investigating the aerosol effects on VIS.

Figure 10 shows the relations between extinction coefficient (EC) and VIS and between SC and VIS by season under different RH levels. Atmospheric VIS is found to decrease exponentially with increasing EC or SC in all seasons. The lapse rate of VIS with EC or SC is much larger in spring and summer than in fall and winter. The lower VIS always appears at higher RH ranges, and vice versa. In small VIS regions (such as: <4 km), VIS values are much smaller in JJA than those in the other seasons under the same SC level, implying the strong effects of RH on VIS. The effect of AAC on VIS has substantial seasonality and it is strong in SON but weak in MAM and JJA as illustrated in the fitting lines in the figure. Study on the effects of PM on VIS might be more reasonable if using the aerosol optical properties rather than its mass concentrations. The linear correlation coefficient between EC and VIS varies from -0.69 (in JJA) to -0.87 (in DJF), and between SC and VIS, it varies from -0.71 (in JJA)

Atmos. Chem. Phys. Discuss., doi:10.5194/acp-2016-420, 2016
Manuscript under review for journal Atmos. Chem. Phys.
Published: 8 August 2016

441 to -0.87 (in DJF) in urban area of Nanjing.

442 **Figure 10**

443 In addition to the SC or EC, the aerosol SSA and ASP also have good relationships with VIS as
444 shown in Figure 11, in which the effects of RH and SAE are also included (larger markers represent
445 smaller SAE, but larger size of the aerosols). The aerosols become coarser, less absorbing and more
446 forward scattering with increasing RH, which subsequently further exacerbate the deterioration of
447 visibility in all the seasons. The linear correlation coefficients vary from -0.48 (in JJA) to -0.73 (in
448 SON) between SSA and VIS and -0.47 (in JJA) to -0.80 (in MAM) between ASP and VIS in urban
449 Nanjing. These results additionally illustrate that the scattering aerosols are still the key factors
450 affecting the atmospheric visibility, although the absorbing aerosols might have considerable influences
451 on VIS in some seasons (Fig. 10c). The results in this study further indicate that effects of aerosols on
452 air quality are complex.

453 **Figure 11**

454 Comparison between surface aerosol extinction coefficient and columnar AOD is performed
455 (Figure 12). Differences exist between EC and AOD, although they are well correlated with each other
456 in each season. AOD to some extent is less affected by the development of boundary layer and more
457 affected by the transport of aerosols compared to EC at the surface. The seasonal mean EC is large both
458 in JJA and in DJF while the largest AOD is only found in JJA, which is possibly related to higher
459 boundary layer height in JJA. A lower boundary layer would lead to more aerosol accumulation at the
460 surface thus result in its smaller column burden. These differences (high surface aerosol loadings but
461 low AOD) have also been simulated by a regional climate chemistry model in Zhuang et al. (2011 and
462 2013). Overall, high AOD level corresponds to large EC value in each season, implying that aerosols in

Atmos. Chem. Phys. Discuss., doi:10.5194/acp-2016-420, 2016
Manuscript under review for journal Atmos. Chem. Phys.
Published: 8 August 2016

463 the upper layers mostly come from surface emissions in urban Nanjing. In some cases, long distance
464 transport of aerosols might contributes significantly to the AOD as shown in Fig. 12a, in which AOD
465 exceeds 2 meanwhile EC is found to appear in low value ranges. The slope of the linear fitting is larger
466 in JJA (about 0.0016) than that in the other seasons (all about 0.001), indicating that for a given value
467 of EC, AOD would be higher in JJA possibly because of higher humidity in summer. The columnar
468 water vapor in summer is about 2 to 5 times of that in the other seasons.

469 **Figure 12**

470 **4 Conclusions**

471 In this study, the near-surface aerosol optical properties, including aerosol scattering (SC), back
472 scattering (Bsp), absorption (AAC) and extinction (EC) coefficients, single scattering albedo (SSA),
473 scattering (SAE) and absorbing (AAE) Ångström exponent, as well as asymmetry parameter (ASP), are
474 investigated based on the measurements with the 7-channel Aethalometer (model AE-31, Magee
475 Scientific, USA) and three-wavelength integrating Nephelometer (Aurora 3000, Australia) in urban
476 area of Nanjing from Mar 2014 to Feb 2016.

477 In urban area of Nanjing, the annual mean EC, SSA and ASP at 550 nm are 381.958 Mm^{-1}, 0.901,
478 0.571, respectively. SC, which accounts for about 90% of EC, is about one order of magnitude larger
479 than AAC, implying that EC to a great degree has similar temporal variation and frequency distribution
480 to SC. Absorbing aerosol is finer than the scattering one. AAE at 470/660 nm is about 1.58, about 0.2
481 larger than SAE. All of them above have substantially seasonal and diurnal variations. Both the aerosol
482 absorption and scattering coefficients have the largest values in winter due to the higher emissions.
483 However, SC also has a higher values in summer and spring likely due to higher relative humidity (RH)
484 and efficiency of gas-to-particle transformation in summer and the effect of dust in spring, respectively.

Atmos. Chem. Phys. Discuss., doi:10.5194/acp-2016-420, 2016
Manuscript under review for journal Atmos. Chem. Phys.
Published: 8 August 2016

485 High RH in summer results in the lowest AAE and largest ASP being found and it is also lead to a
486 relatively smaller SAE, although a large number of fine scattering aerosols could be produced through
487 intensive gas-to-particle transformation in this season. Seasonality of SSA is co-determined by AAC
488 and SC, showing the largest value in summer and lowest value in fall. AAC, SC, Bsp and EC have
489 more substantial diurnal variations than SSA, AAE, SAE and ASP. Because of traffic emissions, AACs
490 are high at the rush hours (around 09:00 am and pm) but low in afternoon when the boundary layer
491 being well developed. SC and Bsp usually peak in the early morning before sunrise (1-2 earlier than
492 AAC's) and reach the bottom in the afternoon. High levels of SC and Bsp are mostly caused by
493 accumulation of air pollution in the nighttime from midnight to sunrise. The diurnal variation of SSA is
494 also depended on AAC and SC. SSA is large after midnight and noon. AAE and SAE at daytime are
495 slightly larger than after midnight because both absorbing and scattering aerosols are fresher at daytime
496 but more aged before sunrise. ASP, which is related to the size of the aerosols, its diurnal variation is
497 opposite to SAE's but similar to Bsp's.

498 Frequency analysis indicates that almost all of the aerosol optical properties follow a unimodal
499 pattern in urban area of Nanjing. The dominant ranges are from 9 to 45 Mm^{-1} for AAC, 60 to 390 Mm^{-1}
500 for SC, 15 to 60 Mm^{-1} for Bsp, 0.87 to 0.97 for SSA 1.4 to 1.8 for AAE, 0.96 to 1.68 for SAE and 0.48
501 to 0.69 for ASP, accounting for more than 73%, 67%, 69%, 73%, 71%, 62% and 81%, respectively, of
502 the total data samples during the entire study period. Frequency distributions of the aerosol optical
503 properties also have substantial seasonality. The frequency peak of a property would be more
504 concentrated among lower/higher ranges if the seasonal mean is smaller/larger. Back trajectory analysis
505 suggests that the source of aerosols in Nanjing are mainly from the local and regional emissions around
506 YRD in summer, while from the sources include both local emissions and transport from central and

Atmos. Chem. Phys. Discuss., doi:10.5194/acp-2016-420, 2016
Manuscript under review for journal Atmos. Chem. Phys.
Published: 8 August 2016

north China in winter. In JJA, aerosols are more scattering when air masses come from the East China Sea and finer if air masses come from remote areas. In DJF, AAC, SC, Bsp, SSA and ASP are low while AAE and SAE are high in urban Nanjing under the conditions of air masses being transported from remote areas. ASP varied with the clusters is consistent with RH in both JJA and DJF.

The correlation between SC and Bsp is much better than that between SC and AAC in all seasons. In spring, these relationships are a little weaker than those in suburban Nanjing. ASP has a quasi-LogNormal distribution with SC under a condition of RH being lower than 60%, increasing monotonically with increasing SC. It would be mostly concentrated at small SC regions when RH is less than 40% because finer particles dominant under low RH conditions. The correlation between ASP and SC becomes weaker with increasing RH, indicating that both fine and coarse aerosols might be equally important to the total SC in high RH conditions. Atmospheric humidity can significantly modulate aerosol optical properties. Due to the effects of RH in summer, the aerosol would become coarser and its forward scattering efficiency would be stronger with increasing in RH. The linear correlation coefficients are -0.36, -0.15 and 0.6 between AAE and RH, SAE and RH, and ASP and RH, respectively, in urban areas of Nanjing. Comparisons also indicate that seasonal variation of surface aerosol EC (high in JJA and DJF) is different from its columnar optical depth (AOD, high in JJA and low in DJF), even though they are closely correlated to each other within each season. Overall, high AOD level corresponding to large EC value in each season implies that aerosols in upper layers are mostly from surface emissions. AOD would be higher in JJA than in other seasons in a condition with fixed EC, possibly due to the effects of high humidity.

Overall, the scattering aerosols are still the key factor in affecting the atmospheric visibility (VIS), although the absorbing aerosol has considerable contributions in some seasons. The linear

correlation coefficient between EC and VIS varies from -0.69 to -0.87, close to those between SC and VIS. VIS is found to be decreased exponentially with increasing EC or SC in all seasons. And its lapse rate along with EC or SC is much larger in spring and summer than in fall and winter. In small VIS regions (i.e., VIS<4 km), VIS values are much smaller in JJA than in other seasons if the SC levels are the same, further indicating the strong effect of RH on VIS. The aerosol SSA and ASP could also affect VIS. Large SSA and ASP might further exacerbate the deterioration of visibility. The linear correlation coefficients between seasonal SSA and VIS varies from -0.48 to -0.73 and from -0.47 to -0.80 between ASP and VIS in urban area of Nanjing.

Acknowledgements: This work was supported by the National Key Basic Research Development Program of China (2014CB441203), the National Natural Science Foundation of China (91544230, 41475122), the New Teachers' Fund for Postdoctoral Fellows, Ministry of Education (20120091120031), FP7 project: REQUA (PIRSES-GA-2013-612671), and a project Funded by the Priority Academic Program Development of the Jiangsu Higher Education Institutions (PAPD). the National Science Foundation of Jiangsu Provence (Grant #BE2015151). The authors would like to thank all members in the AERC of Nanjing University for maintaining instruments. The HYSPLIT model was supplied by NOAA: http://ready.arl.noaa.gov/HYSPLIT_traj.php.

Atmos. Chem. Phys. Discuss., doi:10.5194/acp-2016-420, 2016
Manuscript under review for journal Atmos. Chem. Phys.
Published: 8 August 2016

Atmospheric Chemistry and Physics Discussions

5 References

Andreae, M. O., Schmid, O., Yang, H., Chand, D., Yu, J. Z., Zeng, L. M., and Zhang, Y. H.: Optical properties and chemical composition of the atmospheric aerosol in urban Guangzhou, China Atmos. Environ., 42, 6335–6350, 2008.

Andrews, E., Sheridan, P. J., Fiebig, M., McComiskey, M., Ogren, J. A., Arnott, P., Covert, D., Elleman, R., Gasparini, R., Collins, D., Jonsson, H., Schmid, B., and Wang, J.: Comparison of methods for deriving aerosol asymmetry parameter, J. Geophys. Res., 111, D05S04, doi:10.1029/2004JD005734, 2006.

Arnott, W. P., Hamasha, K., Moosmuller, H., Sheridan, P. J., and Ogren, J. A.: Towards aerosol light-absorption measurements with a 7-wavelength aethalometer: evaluation with a photoacoustic instrument and 3-wavelength nephelometer, Aerosol Sci. Tech., 39, 17–29, doi:10.1080/027868290901972, 2005.

Babu, S., Gogoi, M., Kumar, V. H. A., Nair, V. S., Moorthy, K. K.: Radiative properties of Bay of Bengal aerosols: spatial distinctiveness and source impacts, J. Geophys. Res., 117, D06213, doi:10.1029/2011JD017355, 2012.

Bai, H. T., Chen, Y. H., Wang, H. Q., Zhang, Q., Guo, N., Wang, S., Pan, H., and Zhang, P.: Seasonal variation of aerosol optical properties at AERONET of the semi-arid region in Loess Plateau, Arid Land Geogr., 34, 1–8, 2011.

Bellouin, N., Boucher, O., Tanré, D., and Dubovik, O.: Aerosol absorption over the clear-sky oceans deduced from POLDER-1 and AERONET observations, Geophys. Res. Lett., 30, 1748, doi:10.1029/2003GL017121, 2003.

Bergin, M. H., Cass, G. R., Xu, J., Fang, C., Zeng, L., Yu, T., Salmon, L. G., Kiang, C. S., Tang, X. Y.,

568 Zhang, Y. H., and Chameides, W. L.: Aerosol radiative, physical, and chemical properties in Beijing
569 during June 1999, J. Geophys. Res., 106 (D16), 17969–17980, 2001.
570 Cai, H. K., Zhou, R. J., Fu, Y. F., Zheng, Y. Y., and Wang, Y. J.: Cloud-aerosol lidar with or thogonal
571 polarization detection of aerosol optical properties after a crop burning case, Clim. Environ. Res.,
572 16, 469–478, 2011.
573 Cao, J., Wang, Q., Chow, J. C., Watson, J. G., Tie, X., Shen, Z., Wang, P., and An Z.: Impacts of aerosol
574 compositions on visibility impairment in Xi'an, China, Atmos. Environ., 59, 559–566, 2012.
575 Chameides, W. L., and Bergin, M.: Soot takes center stage, Science, 297 (5590), 2214-2215, 2002.
576 Che, H. Z., Zhang, X. Y., Xia, X., Goloub, P., Holben, B., Zhao, H., Wang, Y., Zhang, X. C., Wang, H.,
577 Blarel, L., Damiri, B., Zhang, R., Deng, X., Ma, Y., Wang, T., Geng, F., Qi, B., Zhu, J., Yu, J., Chen,
578 Q., and Shi, G.: Ground-based aerosol climatology of China: aerosol optical depths from the China
579 Aerosol Remote Sensing Network (CARSNET) 2002–2013, Atmos. Chem. Phys., 15, 7619–7652,
580 2015.
581 Cheng, Y. F., Wiedensohler, A., Eichler, H., Su, H., Gnauk, T., Bruggemann, E., Herrmann, H.,
582 Heintzenberg, J., Slanina, J., Tuch, T., Hu, M., and Zhang, Y. H.: Aerosol optical properties and
583 related chemical apportionment at Xinken in Pearl River Delta of China, Atmos. Environ., 42,
584 6351–6372, 2008.
585 Collaud Coen, M., Weingartner, E., Apituley, A., Ceburnis, D., Fierz-Schmidhauser, R., Flentje, H.,
586 Henzing, J. S., Jennings, S. G., Moerman, M., Petzold, A., Schmid, O., and Baltensperger, U.:
587 Minimizing light absorption measurement artifacts of the Aethalometer: evaluation of five
588 correction algorithms, Atmos. Meas. Tech., 3, 457–474, doi:10.5194/amt-3-457-2010, 2010.
589 Fan, X. H., Chen, H. B., Xia, X. A., Li, Z. Q., and Cribb, M.: Aerosol optical properties from the

590 Atmospheric Radiation Measurement Mobile Facility at Shouxian. China, J. Geophys. Res., 115,
591 D00K33, doi:10.1029/2010JD014650, 2010.
592 Forster, P., Ramaswamy, V., Artaxo, P., Berntsen, T., Betts, R., Fahey, D. W., Haywood, J., Lean, J.,
593 Lowe, D. C., Myhre, G., Nganga, J., Prinn, R., Raga, G., Schulz, M., and Van Dorland, R.: Changes
594 in atmospheric constituents and in radiative forcing, in: Climate Change 2007: The Physical
595 Science Basis. Contribution of Working Group I to the Fourth Assessment Report of the
596 Intergovernmental Panel on Climate Change, edited by: Solomon, S. et al., Cambridge Univ. Press,
597 Cambridge, UK, 129–234, 2007.
598 Gong, W., Zhang, M., Han, G., Ma, X., and Zhu, Z.: An investigation of aerosol scattering and
599 absorption properties in Wuhan, Central China, Atmosphere, 6, 503–520, 2015.
600 He, X., Li, C. C., Lau, A. K. H., Deng, Z. Z., Mao, J. T., Wang, M. H., and Liu, X. Y.: An intensive
601 study of aerosol optical properties in Beijing urban area, Atmos. Chem. Phys., 9, 8903–8915,
602 doi:10.5194/acp-9-8903-2009, 2009.
603 Holler, R., Ito, K., Tohno, S., and Kasahara, M.: Wavelength-dependent aerosol single scattering albedo:
604 measurements and model calculations for a coastal site near the sea of Japan during ACE-Asia, J.
605 Geophys. Res., 108, 8648, doi:10.1029/2002JD003250, 2003.
606 Jacobson, M. Z.: Control of fossil-fuel particulate black carbon and organic matter, possibly the most
607 effective method of slowing global warming, J. Geophys. Res., 107, 4410,
608 doi:10.1029/2001JD001376, 2002.
609 Kiehl, J. T. and Briegleb, B. P.: The relative roles of sulfate aerosols and greenhouse gases in climate
610 forcing, Science, 260, 311–314, 1993.
611 Li, C., Marufu, L. T., Dickerson, R. R., Li, Z., Wen, T., Wang, Y., Wang, P., Chen, H., and Stehr, J. W.:

612 In situ measurements of trace gases and aerosol optical properties at a rural site in northern China
613 during East Asian Study of Tropospheric Aerosols: An International Regional Experiment 2005, J.
614 Geophys. Res., 112, D22S04, doi:10.1029/2006JD007592, 2007.
615 Li, J., Liu, X., Yuan, L., Yin, Y., Li, Z., Li, P., Ren, G., Jin, L., Li, R., Dong, Z., Li, Y., and Yang, J.:
616 Vertical distribution of aerosol optical properties based on aircraft measurements over the Loess
617 Plateau in China, J. Environ. Sci, 34, 44-56, 2015a.
618 Li, J., Yin, Y., Li, P., Li, Z., Li, R., Cribb, M., Dong, Z., Zhang, F., Li, J., Ren, G., Jin, L., and Li, Y.:
619 Aircraft measurements of the vertical distribution and activation property of aerosol particles over
620 the Loess Plateau in China, Atmos. Res., 155, 73–86, 2015b.
621 Li, Z. Q., Lee, K. H., Wang, Y. S., Xin, J. Y., and Hao, W. M.: First observation-based estimates of
622 cloud-free aerosol radiative forcing across China, J. Geophys. Res., 115, D00K18,
623 doi:10.1029/2009JD013306, 2010.
624 Liao, H. and Seinfeld, J. H.: Global impacts of gas-phase chemistry-aerosol interactions on direct
625 radiative forcing by anthropogenic aerosols and ozone, J. Geophys. Res., 110, D18208,
626 doi:10.1029/2005JD005907, 2005.
627 Menon, S., Hansen, J., Nazarenko, L., and Luo, Y. F.: Climate effects of black carbon aerosols in China
628 and India, Science, 297, 2250–2253, doi:10.1126/science.1075159, 2002.
629 Penner, J. E., Andreae, M., Annegarn, H., Barrie, L., Feichter, J., Hegg, D., Jayaraman, A., Leaitch, R.,
630 Murphy, D., Nganga, J., and Pitari, G.: Aerosols, their direct and indirect effects, in: Climate
631 Change 2001: The Scientific Basis. Contribution of Working Group I to the Third Assessment
632 Report of the Intergovernmental Panel on Climate Change, edited by: Houghton, J. T. et al.,
633 Cambridge University Press, Cambridge, UK and New York, NY, USA, 289–348, 2001.

634 Petzold, A., Kopp, C., and Niessner, R.: The dependence of the specific attenuation cross-section on
635 black carbon mass fraction and particle size, Atmos. Environ., 31, 661–672, 1997.
636 Russell, P. B., Kacenelenbogen, M., Livingston, J. M., Hasekamp, O. P., Burton, S. P., Schuster, G. L.,
637 Johnson, M. S., Knobelspiesse, K. D., Redemann, J., Ramachandran, S., and Holben, B.: A
638 multiparameter aerosol classification method and its application to retrievals from spaceborne
639 polarimetry, J. Geophys. Res. Atmos., 119, 9838–9863, doi:10.1002/2013JD021411, 2014.
640 Schmid, O., Artaxo, P., Arnott, W. P., Chand, D., Gatti, L. V., Frank, G. P., Hoffer, A., Schnaiter, M., and
641 Andreae, M. O.: Spectral light absorption by ambient aerosols influenced by biomass burning in the
642 Amazon Basin. I: Comparison and field calibration of absorption measurement techniques, Atmos.
643 Chem. Phys., 6, 3443–3462, doi:10.5194/acp-6-3443-2006, 2006.
644 Streets, D. G., Gupta, S., Waldhoff, S. T., Wang, M. Q., Bond, T. C., and Bo, Y. Y.: Black carbon
645 emissions in China, Atmos. Environ., 35, 4281–4296, doi:10.1016/S1352-2310(01)00179-0, 2001.
646 Tao, J., Zhang, L. M., Cao, J. J., Hsu, S. C., Xia, X. G., Zhang, Z. S., Lin, Z. J., Cheng, T. T., and Zhang,
647 R. J.: Characterization and source apportionment of aerosol light extinction in Chengdu, southwest
648 China, Atmos. Environ., 95, 552–562, 2014.
649 Wang, T. J., Zhuang, B. L., Li, S., Liu, J., Xie, M., Yin, C. Q., Zhang, Y., Yuan, C., Zhu, J. L., Ji, L. Q.,
650 and Han, Y.: The interactions between anthropogenic aerosols and the East Asian summer monsoon
651 using RegCCMS, J. Geophys. Res. Atmos., 120, doi:10.1002/2014JD022877, 2015.
652 Wang, Y., Che, H. Z., Ma, J. Z., Wang, Q., Shi, G. Y., Chen, H. B., Goloub, P., and Hao, X. J.: Aerosol
653 radiative forcing under clear, hazy, foggy, and dusty weather conditions over Beijing, China,
654 Geophys. Res. Lett., 36, L06804, doi:10.1029/2009GL037181, 2009.
655 Weingartner, E., Saathoff, H., Schnaiter, M., Streit, N., Bitnar, B., and Baltensperger, U.: Absorption of

656 light by soot particles: determination of the absorption coefficient by means of aethalometers, J.
657 Aerosol Sci., 34, 1445–1463, doi:10.1016/S0021-8502(03)00359-8, 2003.
658 Wu, D., Mao, J. T., Deng, X. J., Tie, X. X., Zhang, Y. H., Zeng, L. M., Li, F., Tan, H. B., Bi, X. Y.,
659 Huang, X. Y., Chen, J., and Deng, T.: Black carbon aerosols and their radiative properties in the
660 Pearl River Delta region, Sci. China Ser. D, 52, 1152–1163, doi:10.1007/s11430-009-0115-y, 2009.
661 Wu, D.,Wu, C., Liao, B., Chen, H.,Wu, M., Li, F., Tan, H., Deng, T., Li, H., Jiang, D., and Yu, J. Z.:
662 Black carbon over the South China Sea and in various continental locations in South China, Atmos.
663 Chem. Phys., 13, 12257–12270, doi:10.5194/acp-13-12257-2013, 2013.
664 Wu, Y. F., Zhang, R. J., Pu, Y. F., Zhang, L. M., Ho, K. F., and Fu, C. B.: Aerosol optical properties
665 observed at a semi-arid rural site in northeastern China, Aerosol Air Qual. Res., 12, 503–514, 2012.
666 Xia, X. A., Li, Z. Q., Holben, B., Wang, P., Eck, T., Chen, H. B., Cribb, M., and Zhao, Y. X.: Aerosol
667 optical properties and radiative effects in the Yangtze Delta region of China, J. Geophys. Res., 112,
668 D22S12, doi:10.1029/2007JD008859, 2007.
669 Xiao, Z. Y., Jiang, H., Chen, J., Wang, B., and Jiang, Z. S.: Monitoring the aerosol optical properties
670 over Hangzhou using remote sensing data, Acta Sci. Circumst., 31, 1758–1767, 2011.
671 Xu, J., Bergin, M. H., Greenwald, R., Schauer, J. J., Shafer, M. M., Jaffrezo, J. L., and Aymoz, G.:
672 Aerosol chemical, physical, and radiative characteristics near a desert source region of Northwest
673 China during ACE-Asia, J. Geophys. Res., 109, D19S03, doi:10.1029/2003JD004239, 2004.
674 Xu, J., Bergin, M. H., Yu, X., Liu, G., Zhao, J., Carrico, C. M., and Baumann, K.: Measurement of
675 aerosol chemical, physical and radiative properties in the Yangtze delta region of China, Atmos.
676 Environ., 36, 161–173, 2002.
677 Xu, J., Tao, J., Zhang, R., Cheng, T., Leng, C., Chen, J., Huang, G., Li, X., and Zhu, Z.: Measurements

678 of surface aerosol optical properties in winter of Shanghai, Atmos. Res., 109-110, 25–35, 2012.

679 Yan, P., Tang, J., Huang, J., Mao, J. T., Zhou, X.J., Liu, Q., Wang, Z. F., and Zhou, H. G.: The
680 measurement of aerosol optical properties at a rural site in Northern China, Atmos. Chem. Phys., 8,
681 2229–2242, doi:10.5194/acp-8-2229-2008, 2008.

682 Yan, P.: Study on the aerosol optical properties in the background regions in the East part of China,
683 PhD Thesis, Peking University, China, 2006.

684 Yu, X. N., Ma, J., Kumar, K. R., Zhu, B., An, J. L., He, J. Q., and Li, M.: Measurement and analysis of
685 surface aerosol optical properties over urban Nanjing in the Chinese Yangtze River Delta, Sci. Total
686 Environ., 542, 277-291, 2016.

687 Zhang, L., Sun, J. Y., Shen, X. J., Zhang, Y. M., Che, H., Ma, L. Q., Zhang, Y. W., Zhang, X. Y., and
688 Ogren, J. A.: Observations of relative humidity effects on aerosol light scattering in the Yangtze
689 River Delta of China, Atmos. Chem. Phys., 15, 8439–8454, 2015.

690 Zhang, Q., Streets, D. G., Carmichael, G. R., He, K. B., Huo, H., Kannari, A., Klimont, Z., Park, I. S.,
691 Reddy, S., Fu, J. S., Chen, D., Duan, L., Lei, Y., Wang, L. T., and Yao, Z. L.: Asian emissions in
692 2006 for the NASA INTEX-B mission, Atmos. Chem. Phys., 9, 5131–5153,
693 doi:10.5194/acp-9-5131-2009, 2009.

694 Zhang, W., Hu, B., Chen, C. H., Du, P., Zhang, L., and Feng, G. H.: Scattering properties of
695 atmospheric aerosols over Lanzhou City and applications using an integrating nephelometer, Adv.
696 Atmos. Sci., 21(6), 848–856, 2004.

697 Zhang, X. Y., Wang, Y. Q., Niu, T., Zhang, X. C., Gong, S. L., Zhang, Y. M., and Sun, J. Y.:
698 Atmospheric aerosol compositions in China: Spatial/temporal variability, chemical signature,
699 regional haze distribution and comparisons with global aerosols, Atmos. Chem. Phys., 12, 779–799,

700 doi:10.5194/acp-12-779-2012, 2012.

701 Zhu, J., Wang, T., Talbot, R., Mao, H., Hall, C. B., Yang, X., Fu, C., Zhuang, B., Li, S., Han, Y., and
702 Huang, X.: Characteristics of atmospheric Total Gaseous Mercury (TGM) observed in urban
703 Nanjing, China, Atmos. Chem. Phys., 12, 12103–12118, doi:10.5194/acp-12-12103-2012, 2012.

704 Zhuang, B. L., Jiang, F., Wang, T. J., Li, S., and Zhu, B.: Investigation on the direct radiative effect of
705 fossil fuel black-carbon aerosol over China, Theor. Appl. Climatol., 104(3–4), 301–312,
706 doi:10.1007/s00704-010-0341-4, 2011.

707 Zhuang, B. L., Li, S., Wang, T. J., Deng, J. J., Xie, M., Yin, C. Q., and Zhu, J. L.: Direct radiative
708 forcing and climate effects of anthropogenic aerosols with different mixing states over China,
709 Atmos. Environ., 79, 349–361, doi:10.1016/j.atmosenv.2013.07.004, 2013b.

710 Zhuang, B. L., Liu, Q., Wang, T. J., Yin, C. Q., Li, S., Xie, M., Jiang, F., and Mao, H. T.: Investigation
711 on semi-direct and indirect climate effects of fossil fuel black carbon aerosol over China, Theor.
712 Appl. Climatol., 114, 651–672, doi:10.1007/s00704-013-0862-8, 2013a.

713 Zhuang, B. L., Wang, T. J., Li, S., Liu, J., Talbot, R., Mao, H. T., Yang, X. Q., Fu, C. B., Yin, C. Q.,
714 Zhu, J. L., Che, H. Z., and Zhang, X. Y.: Optical properties and radiative forcing of urban aerosols
715 in Nanjing, China, Atmos. Environ., 83, 43–52, 2014a.

716 Zhuang, B. L., Wang, T. J., Liu, J., Li, S., Xie, M., Yang, X. Q., Fu, C. B., Sun, J. N., Yin, C. Q., Liao, J.
717 B., Zhu, J. L., and Zhang, Y.: Continuous measurement of black carbon aerosol in urban Nanjing of
718 Yangtze River Delta, China, Atmos. Environ., 89, 415–424, 2014b.

719 Zhuang, B. L., Wang, T. J., Liu, J., Ma, Y., Yin, C. Q., Li, S., Xie, M., Han, Y., Zhu, J. L., Yang, X. Q.,
720 and Fu, C. B.: Absorption coefficient of urban aerosol in Nanjing, west Yangtze River Delta, China,
721 Atmos. Chem. Phys., 15, 13633–13646, 2015.

Atmos. Chem. Phys. Discuss., doi:10.5194/acp-2016-420, 2016
Manuscript under review for journal Atmos. Chem. Phys.
Published: 8 August 2016

Atmospheric Chemistry and Physics Discussions

Figure captions:

Figure 1. The 10th, 25th, median, 75th, and 90th percentiles of 550 nm AAC (a, Mm^{-1}), 470/660 nm AAE (b), 550 nm SC (c, Mm^{-1}), 550 nm (d, Mm^{-1}) and 450/635 nm SAE (e) in each season from March 2014 to Feburay 2016.

Figure 2. Seasonal means (markers) and corresponding standard deviations (error bars) of wavelength dependent AAC (a, Mm^{-1}), SC (b, solid mark, Mm^{-1}), Bsp (b, open mark, Mm^{-1}), EC (c, Mm^{-1}), SSA (e) and ASP (f) at 450, 532, 550, 635 nm, as well as AAE at 470/660 nm (d, red solid mark) and SAE at 450/635 nm (d, green open mark)

Figure 3. Diurnal variations of 550 nm AAC (a, Mm^{-1}), SC (b, Mm^{-1}), Bsp (c, Mm^{-1}), SSA (d), ASP (g), 470/660 nm AAE (e) and 450/635 nm SAE (f) during the study period.

Figure 4. Frequency (%) distributions of 550 nm AAC (a), SC (b), Bsp (c), SSA (d), ASP (g), 470/660 nm AAE (e) and 450/635 nm SAE (f) on annual (shaded bar) and seasonal (markers in colors) scales.

Figure 5. Clusters of 96-h back trajectories arriving at the study site at 100 m in JJA (a) and DJF (b) simulated by the HYSPIT model. The means with standard deviations of the aerosol optical properties at each cluster of back trajectories in both JJA and DJF are plotted in Fig. 5c and 5d, respectively.

Figure 6. Relationships between 550 nm AAC and SC (solids square in blue) and between 550 nm Bsp and SC (solid cycles in gray) in spring (a), summer (b), autumn (c) and winter (d).

Figure 7. Relationships between the 550 nm ASP and SC in different RH levels.

Figure 8. Relationships between the 491 nm SSA and extinction Angstrom exponent (EAE) at 491/863 nm (a) and between the SSA difference (863-491 nm) and EAE at 491/863 nm (b).

Figure 9. Seasonal variations of RH (a, %) and linear correlations between AAE and RH (b, light blue, upper), between SAE and RH (b, green, middle), and between ASP and RH (c, deep blue, lower).

Atmos. Chem. Phys. Discuss., doi:10.5194/acp-2016-420, 2016
Manuscript under review for journal Atmos. Chem. Phys.
Published: 8 August 2016

Atmospheric Chemistry and Physics Discussions

744 Figure 10. Relationships between SC and visibility (open cycles) and between EC and visibility (solid
745 cycles) in different RH levels in spring (a), summer (b), autumn (c) and winter (d).
746 Figure 11. Relationships between SSA and visibility (solid cycles) and between ASP and visibility
747 (solid squares) in different RH and AAE levels in spring (a), summer (b), autumn (c) and winter (d).
748 Figure 12. Relationships between surface EC at 550 nm and column AOD at 500 nm in spring (a),
749 summer (b), autumn (c) and winter (d).
750
751 **Table captions:**
752 Table 1 Statistical summary of the surface aerosol optical properties in Nanjing.
753 Table 2 Seasonal mean±SD of the surface aerosol optical properties in Nanjing.
754 Table 3 The aerosol optical properties in Nanjing and at other sites of China.
755
756

Atmos. Chem. Phys. Discuss., doi:10.5194/acp-2016-420, 2016
Manuscript under review for journal Atmos. Chem. Phys.
Published: 8 August 2016

Atmospheric Chemistry and Physics Discussions

757 Table 1 Statistical summary of the surface aerosol optical properties in Nanjing

Factors	Max	Min	Mean±SD	Median
550 nm AAC (Mm^{-1})	230.648	1.439	29.615±20.454	24.572
550 nm SC (Mm^{-1})	2493.092	20.673	338.275±228.078	284.379
550 nm Bsp (Mm^{-1})	300.101	1.401	44.257±27.396	38.206
550 nm EC (Mm^{-1})	2643.101	31.186	381.958±252.271	321.679
550 nm SSA	0.988	0.404	0.901±0.049	0.908
550 nm ASP	0.908	0.118	0.571±0.088	0.582
470/660 nm AAE	3.256	0.145	1.583±0.228	1.592
450/635 nm SAE	3.344	0.162	1.320±0.407	1.317

758 AAC: Aerosol absorption coefficient

759 SC: Aerosol scattering coefficient

760 Bsp: Aerosol back scattering coefficient

761 SSA: Aerosol single scattering albedo

762 ASP: Aerosol asymmetry parameter

763 AAE: Ångström exponent of absorbing aerosols

764 SAE: Ångström exponent of scattering aerosols

765

766 Table 2 Seasonal mean±SD of the surface aerosol optical properties in Nanjing

Factors	MAM	JJA	SON	DJF
550 nm AAC (Mm^{-1})	26.954±18.632	19.653±15.689	33.474±19.686	37.958±21.892
550 nm SC (Mm^{-1})	318.998±202.264	340.865±226.151	294.624±200.052	385.137±255.282
550 nm Bsp (Mm^{-1})	42.995±23.580	36.990±25.067	38.684±23.017	54.786±30.974
550 nm EC (Mm^{-1})	341.279±209.315	370.236±248.125	351.887±244.267	422.569±273.565
550 nm SSA	0.915±0.043	0.933±0.049	0.874±0.053	0.890±0.040
550 nm ASP	0.553±0.086	0.638±0.069	0.566±0.079	0.540±0.083

Atmos. Chem. Phys. Discuss., doi:10.5194/acp-2016-420, 2016
Manuscript under review for journal Atmos. Chem. Phys.
Published: 8 August 2016

Atmospheric Chemistry and Physics Discussions

470/660 nm AAE	1.571±0.172	1.488±0.263	1.524±0.277	1.701±0.156
450/635 nm SAE	1.097±0.320	1.337±0.428	1.544±0.352	1.235±0.383

767

Atmos. Chem. Phys. Discuss., doi:10.5194/acp-2016-420, 2016
Manuscript under review for journal Atmos. Chem. Phys.
Published: 8 August 2016

Atmospheric Chemistry and Physics Discussions

768 Table 3 The aerosol optical properties both in Nanjing and at other sites of China

Site	Period	AAC (Mm^{-1})	SC (Mm^{-1})	ASP	SSA	Method	References
Nanjing (urban)	2014.3-2016.2	29.6 (550 nm)	338.3 (550 nm)	0.57 (550 nm)	0.9 (550 nm)	[a] AE-31 [b] Aurora 3000	This stuty
Beijing (urban)	2005-2006	56 (532 nm)	288 (525 nm)	/	0.8 (525 nm)	[c] AE-16 [d] M9003	He et al. (2009)
Beijing (rural)	2003-2005	17.5 (525 nm)	174.6 (525 nm)	/	0.88 (525 nm)	[a] AE-31 [d] M9003	Yan et al. (2008)
Xi'an (urban)	2009	/	525 (520 nm)	/	/	[e] Auroral 1000	Cao et al. (2012)
Chengdu (urban)	2011	96 (532 nm)	456 (520 nm)		0.82	[a] AE-31 [f] Aurora 1000G	Tao et al. (2014)
Wuhan (urban)	2009.12-2014.03	119 (520 nm)	377 (550 nm)	/	0.73 (520 nm)	[a] AE-31 [g] Model 3563	Gong et al. (2015)
Xinken (rural)	2004.10-2011.05	70 (550 nm)	333 (550 nm)	/	0.83 (550 nm)	[h] MAAP [g] Model 3563	Cheng et al. (2008)
Tongyu (rural)	Spring, 2010 Spring, 2011	7.61 (520 nm) 7.01 (520 nm)	89.2 (520 nm) 85.3 (520 nm)	/ /	0.9 (520 nm)	[a] AE-31 [b] Aurora 3000	Wu et al. (2012)
Nanjing (suburban)	2011.03-04	28.1 (532 nm)	329.3 (550 nm)	/	0.89 (532 nm)	[i] PASS [d] Model 3563	Yu et al. (2016)
Shanghai (ruban)	2010.12-2011.03	66 (532 nm)	293 (532 nm)	/	0.81 (532 nm)	[a] AE-31 [g] Model 3563	Xu et al. (2012)
Shouxian (rural)	2008.5-12	29 (550 nm)	401 (550 nm)	/	0.92 (550 nm)	[j] Model PSAP [g] Model 3563	Fan et al. (2010)
Lanzhou (urban)	Winter 2001, 2002	/	226 (550 nm)	/	/	[d] Model 3563	Zhang et al. (2004)
Panyu (urban)	Spring and winter, 2008	84.03 and 188.8 (532 nm)	/	/	/	[a] AE-31	Wu et al. (2013)
Dongguan (suburban)	Spring and winter, 2008	47.1 and 95.53 (532 nm)	/	/	/	[a] AE-31	Wu et al. (2013)

Atmos. Chem. Phys. Discuss., doi:10.5194/acp-2016-420, 2016
Manuscript under review for journal Atmos. Chem. Phys.
Published: 8 August 2016

Atmospheric Chemistry and Physics Discussions

Maofengshan (Rural)	Spring and winter, 2008	26.45 and 28.77 (532 nm)	/	/	/	[a] AE-31	Wu et al. (2013)
Yongxing Island	Spring and winter, 2008	7.21 and 8.37 (532 nm)	/	/	/	[a] AE-31	Wu et al. (2013)

[a] Seven channels Aethalomter (model AE-31, Magee Scientific, USA)

[b] Three wavelength integrating Nephelometer (Model Aurora 3000, Australia)

[c] Aethalometer AE16

[d] Nephelometer M9003

[e] Integrating Nephelometer (Model Aurora 1000)

[f] Integrating Nephelometer (Model Aurora 1000G)

[g] Integrating Nephelometer (Model 3563, TSI, USA)

[h] Multi-angle Absorption Photometer (MAAP, Thermo, Inc., Waltham, MA USA, Model 5012)

[i] Photo acoustic Soot Spectrometer (PASS 1, DMT, USA)

[j] Particle/SootAbsorption Photometer

Atmos. Chem. Phys. Discuss., doi:10.5194/acp-2016-420, 2016
Manuscript under review for journal Atmos. Chem. Phys.
Published: 8 August 2016

Atmospheric Chemistry and Physics Discussions

780 **Figures:**

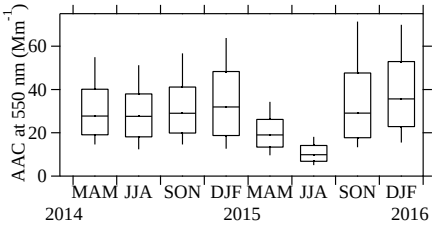

781
782 a)

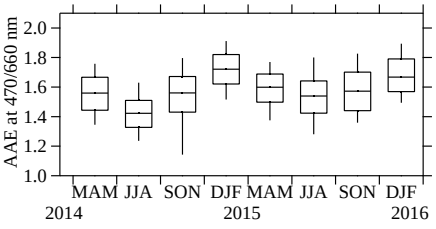

783
784 b)

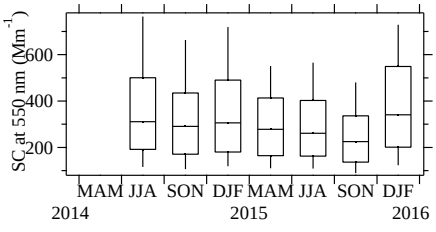

785
786 c)

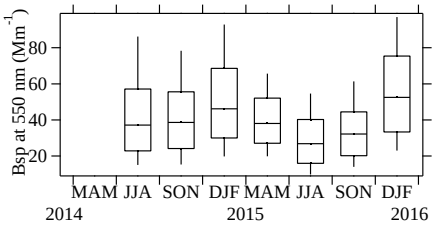

787
788 d)

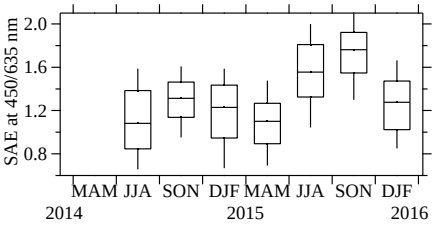

789
790 e)
791 Figure 1.
792

Atmos. Chem. Phys. Discuss., doi:10.5194/acp-2016-420, 2016
Manuscript under review for journal Atmos. Chem. Phys.
Published: 8 August 2016

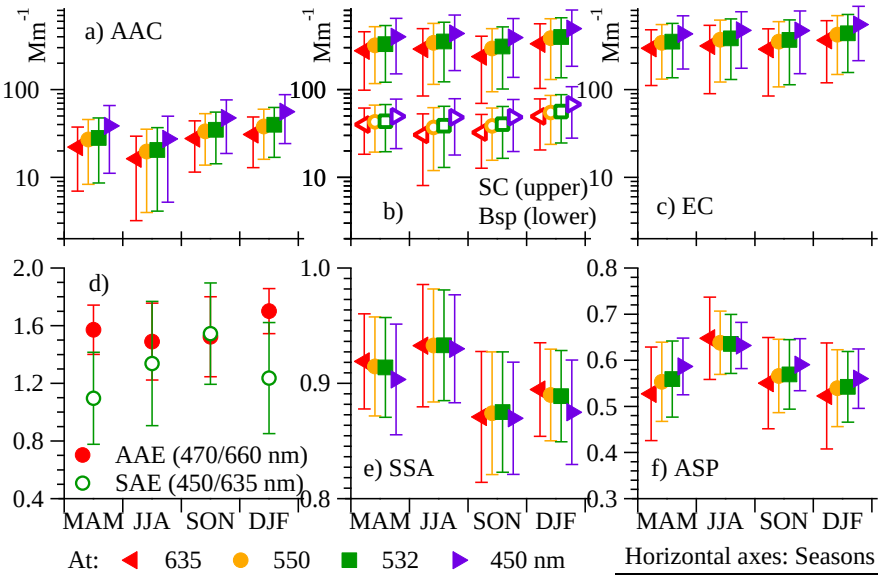

Figure 2.

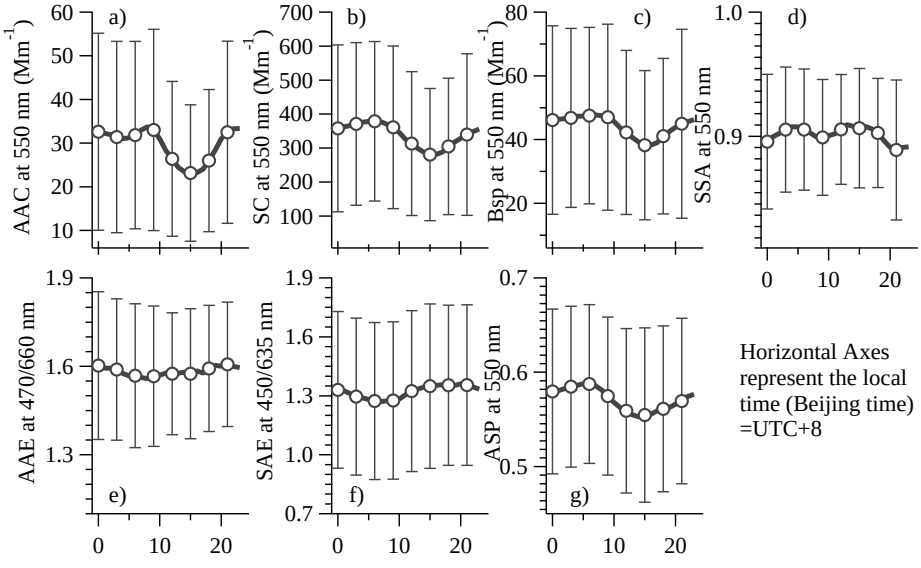

Figure 3

Atmos. Chem. Phys. Discuss., doi:10.5194/acp-2016-420, 2016
Manuscript under review for journal Atmos. Chem. Phys.
Published: 8 August 2016

Atmospheric Chemistry and Physics Discussions

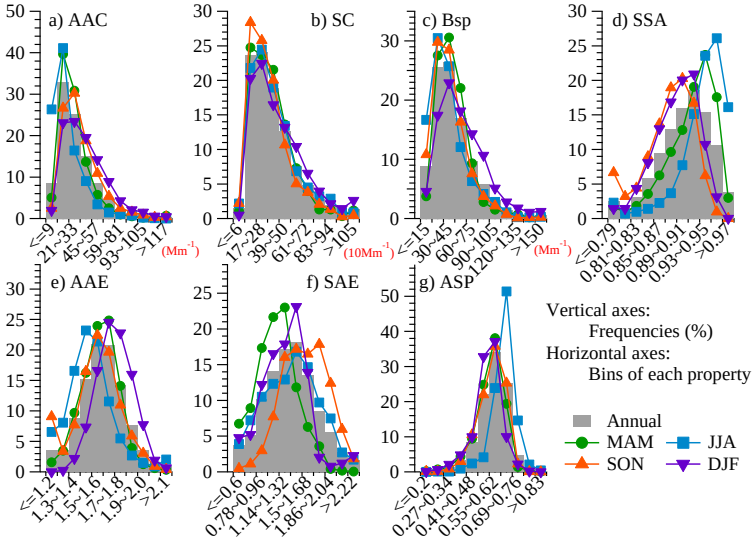

Figure 4

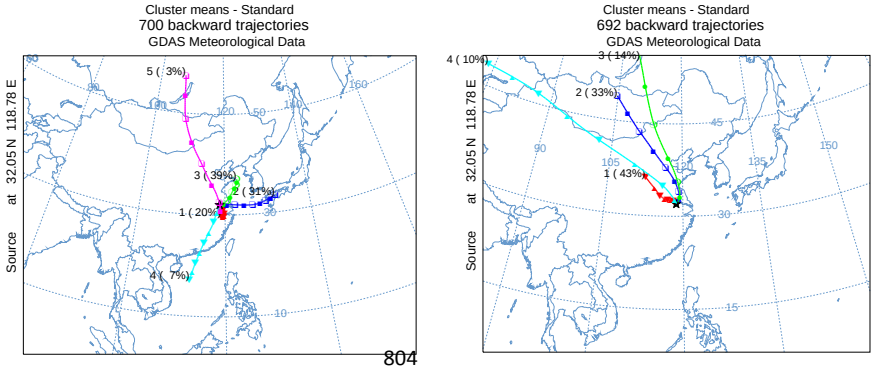

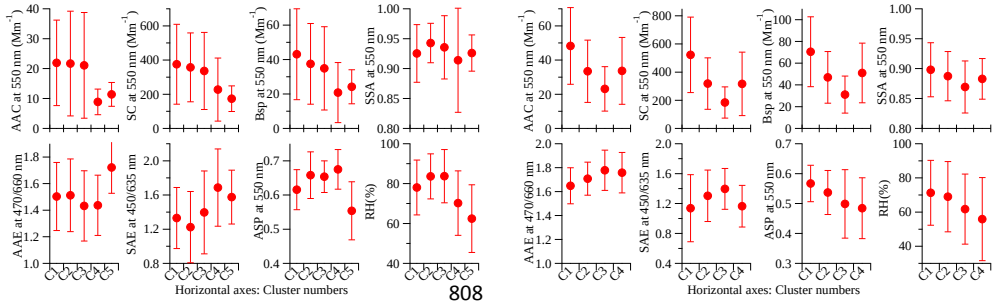

Figure 5

Atmos. Chem. Phys. Discuss., doi:10.5194/acp-2016-420, 2016
Manuscript under review for journal Atmos. Chem. Phys.
Published: 8 August 2016

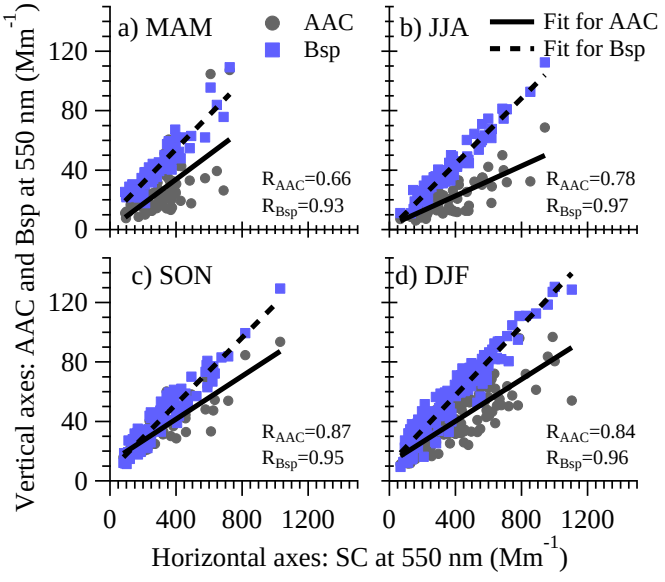

Figure 6

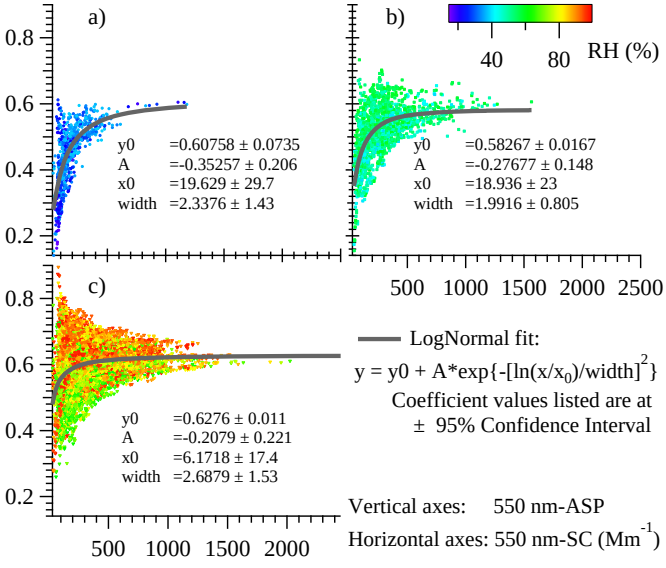

Figure 7

Atmos. Chem. Phys. Discuss., doi:10.5194/acp-2016-420, 2016
Manuscript under review for journal Atmos. Chem. Phys.
Published: 8 August 2016

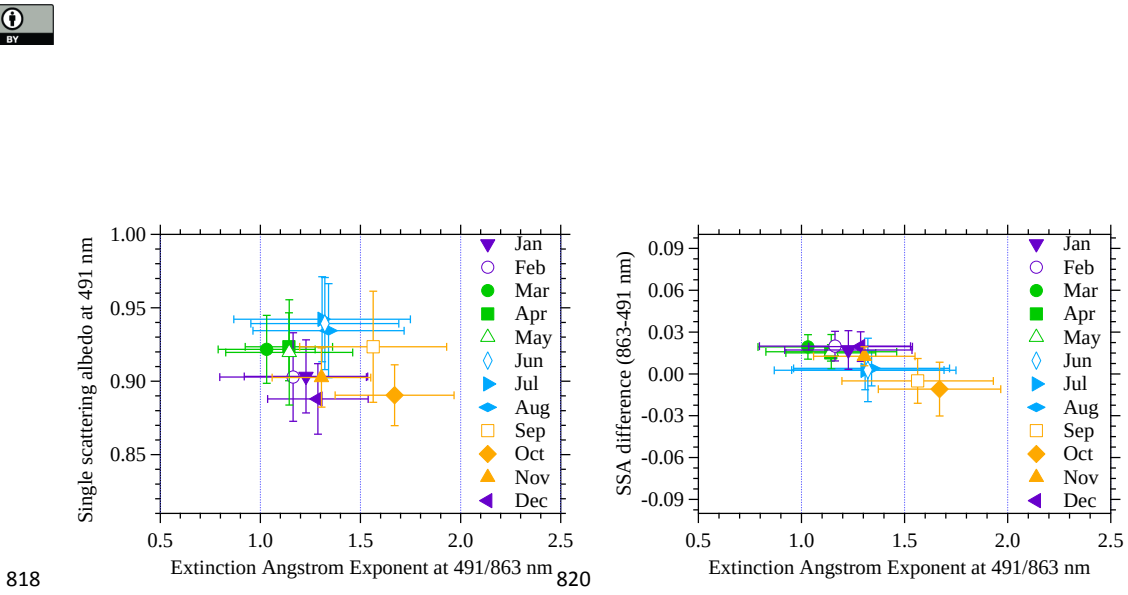

a) b)

Figure 8

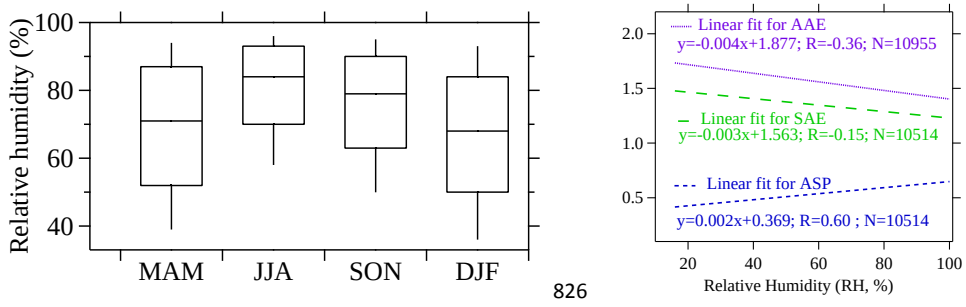

a) b)

Figure 9

Atmos. Chem. Phys. Discuss., doi:10.5194/acp-2016-420, 2016
Manuscript under review for journal Atmos. Chem. Phys.
Published: 8 August 2016

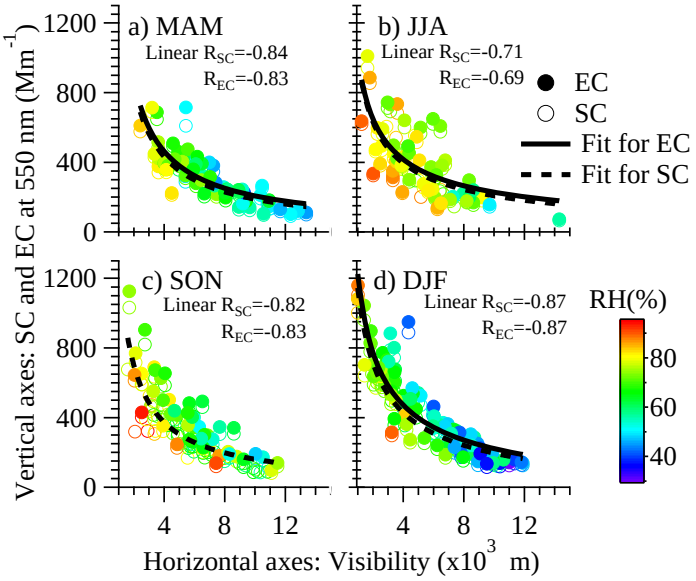

Figure 10

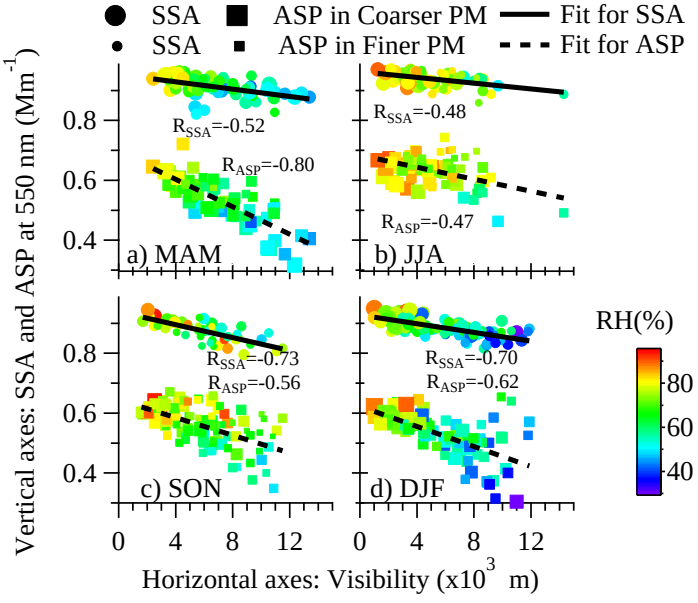

Figure 11

Atmos. Chem. Phys. Discuss., doi:10.5194/acp-2016-420, 2016
Manuscript under review for journal Atmos. Chem. Phys.
Published: 8 August 2016

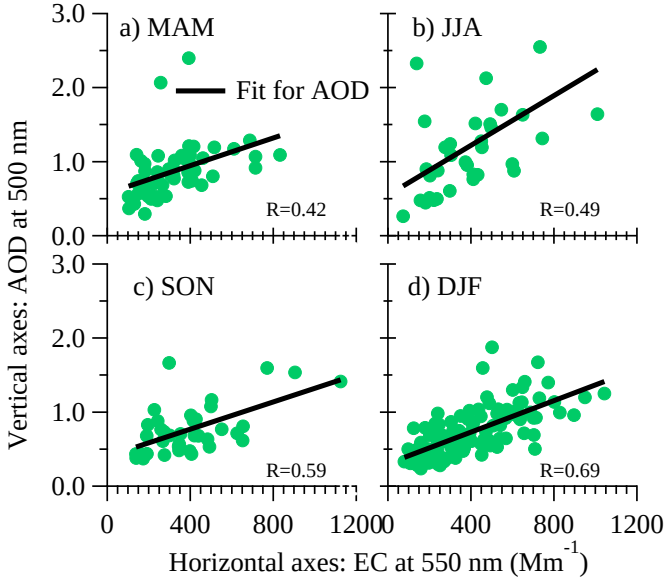

835

836 Figure 12